Applied Surface Science 387 (2016) 317–331

Contents lists available at ScienceDirect

Applied Surface Science

journal homepage: www.elsevier.com/locate/apsusc

Controlled assembly of silver nano-fluid in *Heliotropium crispum* extract: A potent anti-biofilm and bactericidal formulation

Faria Khan [a], Muhammad Uzair Hashmi [a], Nauman Khalid [b,c,d,e,**], Muhammad Qasim Hayat [f], Aamer Ikram [g], Hussnain A. Janjua [a,*]

[a] *Department of Industrial Biotechnology, Atta-ur-Rahman School of Applied Biosciences, National University of Science and Technology, Islamabad 44000, Pakistan*
[b] *Food Engineering Division, National Food Research Institute, NARO, 2-1-12 Kannondai, Tsukuba, Ibaraki 305-8642, Japan*
[c] *Graduate School of Life and Environmental Sciences, University of Tsukuba, 1-1-1 Tennoudai, Tsukuba, Ibaraki 305-8572, Japan*
[d] *The Alliance for Research on North Africa (ARENA), University of Tsukuba, 1-1-1 Tennoudai, Tsukuba, Ibaraki 305-8577, Japan*
[e] *School of Agriculture, University of Management and Technology, Lahore, Pakistan*
[f] *Medicinal Plants Research Laboratory, Department of Plant Biotechnology, Atta-ur-Rahman School of Applied Biosciences, National University of Sciences and Technology, Islamabad 44000, Pakistan*
[g] *Department of Microbiology, Armed Forces Institute of Pathology, Rawalpindi, Pakistan*

ARTICLE INFO

Article history:
Received 23 December 2015
Received in revised form 13 May 2016
Accepted 24 May 2016
Available online 27 May 2016

Keywords:
Silver nanoparticles
Anti-biofilm agents
Heliotropium crispum
Synthesis
Bactericidal effect
Green synthesis

ABSTRACT

The study describes the optimized method for silver nanoparticle (AgNPs) synthesis using *Heliotropium crispum* (HC) plant extract. Optimization of physicochemical parameters resulted in stable and rapidly assembled AgNPs. FTIR results suggest presence of plant phytochemicals that helped in the reduction, stabilization and capping of AgNPs. The assembled Ag nano-composites displayed the peak surface plasmon resonance (SPR) around 428 nm. The presence of uniquely assembled Ag-biomolecule composites, cap and stabilize nanoparticles in aqueous plant suspension. Spherical, uniform-shaped AgNPs with low poly-dispersion and average particle size of 42 nm and was determined through dynamic light scattering (DLS) and scanning election microscopy (SEM) which present robust interaction with microbes. The study also evaluates the antimicrobial and anti-biofilm properties of biologically synthesized AgNPs on clinical isolates of MRSA, *Pseudomonas aeruginosa* and *Acinetobacter baumannii*. Minimum inhibitory concentration (0.5 mg mL^{-1}) of nanoparticles that presented bactericidal effect was made through inhibition assays on bacterial strains. The concentration which presented potent bactericidal response was then evaluated through growth inhibition in liquid medium for anti-biofilm studies at 2.0 mg mL^{-1}. HC-Ag nanoparticles mediated anti-biofilm effects on *Pseudomonas aeruginosa* was revealed through SEM. Complete breakdown of biofilm's extracellular polymeric substances resulted after incubation with AgNPs. Peptidoglycan cell wall destruction was also revealed on planktonic bacterial images after 24 h of incubation.

1. Introduction

Metallic silver (Ag) as assembled nano-composites confer broad-spectrum bactericidal and anti-biofilm responses against multiple drug resistant (MDR) bacterial species. Ag nanoparticles (AgNPs) have established anti-microbial effects; products include wound dressings, paints, food containers, textile products, disinfectant sprays, water sanitizer agent and as a catheter coat [1–3]. The biocidal activity of AgNPs is dependent upon various factors such as size, shape, surface coatings, ionized form of final product and overall nanoparticles charge [4].

The exact antimicrobial mechanism of AgNPs is not known, however, it is proposed to confer damage on bacterial cell wall and cause interaction with thiol groups in enzymes, disrupting bacterial respiratory chain by generating reactive oxygen species (ROS), which can lead to oxidative stress and cell damage [5]. Ag nanocomposites in immobilized form also confer predominant antimicrobial activity through controlled release of Ag^{+} from fine AgNPs composite [4]. It is hence suggested that AgNPs interaction with bacterial cells is extremely robust due to nano-metric dimensions providing potent anti-bacterial effect [5]. Such interactions become more

* Corresponding author.
** Corresponding author at: The Alliance for Research on North Africa (ARENA), University of Tsukuba, 1-1-1 Tennoudai, Tsukuba, Ibaraki 305-8577, Japan.
E-mail addresses: khalid.nauman.ge@u.tsukuba.ac.jp (N. Khalid), hussnain.janjua@asab.nust.edu.pk, janjua.hussnain@gmail.com (H.A. Janjua).

http://dx.doi.org/10.1016/j.apsusc.2016.05.133
0169-4332/

pronounced when nano-composites exhibit size of 10–40 nm, as now the nanoparticles enters dimension of biological macromolecules such as nucleic acids and some proteins [6]. The surface area of synthesized nanomaterials can increase their biological efficacy due to increased surface energy of assembled nanoparticles [7]. AgNPs confer potent anti-biofilm response by destroying hydrated polymeric matrix in cell wall; the anti-biofilm potential is also noted to be species independent hence it is quiet beneficial for futuristic nano-Ag applications to control the spread of resistant microbes [8,9].

Biological synthesis of nanoparticles has opened up the possibility for "green synthesis" which saves cost and energy for synthesis of nano-materials. The overall synthesis process is environmentally benign with great potential towards "application research" of nanomaterials [4,6]. Biological nanoparticles have also been found to be more biocompatible for therapeutic and medicinal application due to the simple synthesis procedure, which eliminates the use of hazardous chemical and also provides ease for scalability of final product [4,6]. Non-toxic, safe, environment friendly and controlled synthesis of nanoparticles have a unique compositional assembly, dependent upon the type of biological source selected [7]. Plant system is the most commonly used biological mode for nanomaterial synthesis and various plant species have already been studied for antibacterial AgNPs synthesis [4].

Plant extract has strong reduction potential (as enzymes, phytochemicals, protein-derived functional groups and vitamins) which can reduce Ag^+ to Ag nano assembly. Control over physicochemical parameters such as concentration, temperature and pH during self-assembly process can further contribute to stability of assembled nanoparticles. Various plant derived extracts contain biological functional groups which can provide novel pharmacophore active compounds to nano-fluid and result in overall stability of the nanocomposites [10].

Biological synthesis of silver nanoparticles using various plant extracts have already been reported. Previous studies suggest size and shape dependent control of nanoparticles synthesis by varying biomaterials. In one study *Ocimum tenuiflorum*, *Solanum tricobatum*, *Syzygium cumini*, *Centella asiatica* and peels of *Citrus sinensis* extracts were utilized as reducing agents to obtain average size range of AgNPs between 40 and 50 nm. The observed antibacterial effects of AgNPs were dependent upon plant extract which provide reduction and capping of AgNPs [8]. Similarly, Song and Kim [9] reported rapid and ecofriendly synthesis of AgNPs in which varying reaction conditions altered the size of nanoparticles. *Aloe vera* plant extract mediated AgNPs exhibited 20 nm size, *Menthapiperita* extract exhibits size of 90 nm, Latex of *Jatrophacurcas* nanoparticles have size of 20 nm and Papaya fruit extract mediated AgNPs have size range of 10–50 nm [10–13]. However, none of the previous studies reported physicochemical optimization of AgNPs synthesis for rapid and cost-efficient synthesis. Moreover, their detailed mode of anti-bacterial and anti-biofilm effects in clinical MDR strains were not reported.

In current research biosynthesis of AgNPs in *Heliotropium crispum* plant extract was demonstrated. To our knowledge, there are no reports of *Heliotropium* sp. mediated synthesis of AgNPs before. We selected the herbal plant for the antibacterial AgNPs synthesis on the evidence of its burn soothing, boils diminishing and wound healing powers in traditional medicine [14]. The plant species *Heliotropium* is used as an aqueous paste for anti-bacterial, anti-fungal, anti-infectious and anti-malarial agents [15]. It has strong wound healing and anti-inflammatory properties which can be incorporated in the nano-fluid during nanoparticle synthesis for pronounced anti-infection effects as the pharmacological-active components present in extract can be incorporated in assembled nano-fluid. Belonging to Boraginaceae family, *Heliotropium crispum* is constituted by pyrrolizidine alkaloids, metabolites which are chemically and biologically reactive and tend to undergo biotransformation [16]. Alkaloids are hydrolysed and oxidized, a phenomenon which can help in the reduction of Ag^+ to Ag during the Alkaloids biotransformation process and at the same time, eliminating the toxicity associated with pyrrolizidine alkaloids [17,18]. The dispersed assembled Ag nanoparticles in current study exhibited controlled morphology and average particle size of 42 nm. The unique compositional assembly of Ag nano-fluid was then tested for anti-biofilm and antibacterial potential with detailed study on exact mode of bactericidal actions up to 72 h of administration in bacterial broth.

2. Material and methods

2.1. Nanoparticle synthesis and characterization

2.1.1. Plant collection and identification

Heliotropium crispum (Fig. S1) was obtained from Medicinal Plants Department at Atta-ur-Rahman Institute of Biological Sciences, National University of Science and Technology, Islamabad, Pakistan which was collected from Cholistan Desert, Pakistan. Identification of plants was carried out on the basis of visible features and characteristics such as stem thickness, nutlet margin, leaf margin and presence of hairs etc. using Tropicos® online database [17] (Table S1).

2.1.2. Preparation of aqueous plant extract

Whole plant was washed with distilled water to remove any impurities and allowed to dry at ambient temperature. Later dried plants were chopped (Royaline, Pakistan) to small size and crushed into a powder. The powder was passed through a sieve mesh no. 80 (Royaline, Pakistan) and fine powder of size $\leq$180 μm was collected to obtain fine suspension in extract. 0.5 g of powder was weighed and added to 100 mL of deionized water. Similarly, 1.0 g and 1.5 g of powder were weighed separately and added to 100 mL of deionized water to get three final concentrations of 50 mg mL^{-1}, 100 mg mL^{-1} and 150 mg mL^{-1} of plant extracts respectively. The plant extracts were boiled for two min and allowed to cool down at ambient temperature. Finally, the cooled extracts were filtered through Whatman Filter Paper 1 (pore size 0.44 μm) and again through syringe filter (0.2 μm) (Milex, Germany) to obtain fine clear aqueous plant extract of light yellow color. The plant extracts were stored in refrigerator at 4 °C for further use.

2.1.3. Synthesis of nanoparticles

The aqueous solution of 1 mM silver nitrate ($AgNO_3$) was prepared by dissolving $AgNO_3$ powder (Riedel de Haen, Germany) in deionized water for synthesis of AgNPs. 0.3 mL of 50 mg mL^{-1} concentration of plant extract was selected and added to 10 mL of 1 mM $AgNO_3$ solution. The tube was placed in magnetic stirrer (Velp-Scientifica, Europe) for 3 h at 37 °C, to allow complete reaction of extract with $AgNO_3$. Here, the plant filtrate act as a reducing and capping agent for Ag^+ reduction in $AgNO_3$ solution. Preliminary confirmation of synthesis of AgNPs was made through color change in the reaction mixture from colorless to light yellow and finally to yellowish-brown within 30 min. To achieve maximum yield and attain stability, nanoparticles were allowed to react for 2 h.

2.1.4. Physicochemical optimization through surface plasmon resonance

AgNPs were characterized initially by monitoring their surface plasmon resonance (SPR) and absorption spectrum in UV–vis spectra on spectrophotometer (Perkin Elmer, Lamda 35). The scanning range of sample was in between 300 and 700 nm with the sampling interval of 1 nm. Base line correction of spectrophotometer

was carried out by using deionized water as a blank. UV–vis spectra of plant extract was also recorded to confirm that the absorption peak with corresponding wavelengths are a result of reduction of metal ions to nanoparticles after addition of $AgNO_3$ to plant extract. Recorded UV visible spectra of samples were then analyzed as a numerical data plotted on Origin-Pro 8.0 software. For optimization of AgNPs according to substrate concentration, different molarities of $AgNO_3$ solutions were prepared (1–5 mM, respectively). 10 mL of each molar $AgNO_3$ solution was taken and allowed to react with 0.1 mL of 50 mg mL^{-1} of plant extract. Each reaction mixture was allowed to incubate overnight at 37 °C. In order to observe the effect of varying concentrations of plant extract on reduction and capping of AgNPs, different dilutions of plant extracts (50 mg mL^{-1}, 100 mg mL^{-1} and 150 mg mL^{-1}) were allowed to react with a 10 mL of 1 mM $AgNO_3$. The concentration of each plant dilution was further varied by adding 0.1–0.5 mL of extract to 1 mM $AgNO_3$. AgNPs were also optimized by varying pH of reaction mixture. The pH of reaction mixture was varied by adding 1 mM HCl for acidic pH and 1 mM of NaOH for basic pH of reaction mixture, pH was recorded via pH meter (Ino Lab, WTW series, Germany). The reaction mixture was also placed overnight at 20–80 °C respectively.

2.1.5. Atomic force microscopy (AFM) studies

Glass slides were cut equally to 1 cm^2 and functionalized by rinsing with 100% ethanol, acetone and deionized water in sequential steps for 1–2 min. The slides were picked with sterile forceps and air dried in clean sterilized place. 50 μL of AgNPs samples were taken from pipette and diluted in 5 mL of de ionized water. Drop of homogenized sample was dropped unto cut glass slides and dried under UV-lamp for 15 min before finally loaded into Scanning Probe for AFM analysis. Both 2D and 3D images of bio-synthesized silver nanoparticles were obtained using Scanning Probe Microscopy, model no JSPM-5200 (Joel, USA). Analysis of AFM images was performed using Scanning Probe Image Processor (SPIP) 6.2.8 software. Several parameters including diameter, area, *z*-range and contour heights were analyzed for nanoparticles.

2.1.6. Scanning electron microscope studies

Scanning electron microscopic (SEM) analysis was carried out using analytical low vacuum SEM (Jeol) model no JSM-6490LA, Japan. Automated vacuum change-over mode was selected for this study. Accelerating voltage of microscope range was set at 20 kV for each sample. 50 μL of colloidal nanoparticle solution was pipetted in almost 5 mL of de-ionized water. Diluted nanoparticle solution was sonicated in an ultra-sonicator (Cole-Parmer 8890, USA), drop of homogenized samples was dropped unto 1 cm^2 glass slides and dried under UV-lamp for 15 min. The samples were sputter coated with gold to make them conductive and mounted for SEM analysis. Images at different magnification and resolution were captured for characterization of nanoparticles.

2.1.7. Energy dispersive X-ray spectroscopy (EDS) studies

The Energy Dispersive X-ray Spectroscopy normally reveals the presence of phases in samples. Compositional analysis on the samples was carried out by the energy dispersive EDS attached with the SEM. The EDX analysis of Ag sample was done by SEM (JSM-6490LA-JEOL) machine. Accelerating Voltage of machine was set at 20.0 kV with probe current of 1.000 nA. PHA mode T_3 was selected with real time 56.03 s and live time of 50.00 s for the analyser. Counting rate was 2785 counts per second (cps) for Ag samples while energy range was selected between 0 and 20 keV for both the samples.

2.1.8. Particle size distribution and zeta potential analysis

Zeta-potential measurements were performed on a Malvern Zetasizer Nano-ZSP at 25 °C with an incident wavelength of 633 nm and a 173° backscattering angle. Clear disposable zeta-potential cells (1 cm path length) were rinsed with ethanol, followed by deionized water prior to sample loading. The viscosity, refractive index, and absorption values were provided in the Malvern software for water (μ = 0.8872 cP, RI = 0.135) and crystalline silver (RI = 1.3330, absorption = 3.987). Twenty runs were averaged for each liquid sample for accurate determination of zeta-potential measurements.

2.1.9. Fourier transform infrared spectroscopy (FTIR)

Perkin-Elmer Spectrum-100 FTIR Spectrometer, USA was used in the present study, whereby scanning was carried out by wavelength in the region 450–4000 cm^{-1} with a resolution of 1 cm^{-1}. Potassium Bromide (KBr) has hygroscopic properties and it was heated to 110 °C to remove the traces of water prior to sample loading. Pellet of KBr was prepared using hydraulic press of plant extract and AgNPs and IR waves passing through each sample. Detected functional groups as a function of %age transmission with corresponding wavenumbers graph was plotted.

2.2. Antibacterial activity of silver nanoparticles

2.2.1. Collection of bacterial strains

Strains of Multiple Drug Resistant Gram Negative *Pseudomonas aeruginosa* (PA) and *Acinetobacter baumanii* (AB) and Gram Positive Multiple Drug Resistant *Staphylococcus aureus* (MRSA) were collected from Armed Forces Institute of Pathology (AFIP), Rawalpindi, Pakistan. The isolated bacterial strains were growing in differential media (Mc Conkey and Blood Agar). Antibiotic resistance profile was checked for each of the collected strains and diameter size of an inhibition zone was marked as either Resistant (R), Sensitive (S) or Intermediate (I) for each antibiotic (Table S3) using standard susceptibility zone for antibiotic as recorded in Table S2, S4 and S5. The bacterial strains collected were stored in 87% glycerol stock solution and vials were stored at −80 °C.

2.2.2. Preparation of nanoparticles concentration

1.5 mL of AgNPs solution was added in eppendorf tube and allowed to centrifuge at 14800 rpm (Concentrator Plus, Germany) for time span of 1 h. A brown pellet of nanoparticles was obtained at bottom of tube while clear transparent supernatant was discarded from the top, the pellet obtained was washed with acetone, centrifuged and supernatant discarded. The pellet was allowed to dry at 37 °C incubator for 16 h with cap left open. Different concentrations of AgNPs were prepared for their antibacterial activities. Purified dried nanoparticles powder was weighed and dissolved in deionized water by vortexing at speed of 2000 rpm (VelpScientifica, Europe), followed by sonication for one hour prior to use. The concentrations of AgNPs ranged from 0.25 to 2.0 mg mL^{-1}.

2.2.3. Antibacterial disk diffusion assay

McConkey agar (Merk) and nutrient agar (Merk) were prepared in distilled water and autoclaved prior to use. The agars were poured into autoclaved petri plates inside the laminar flow hood cabinet (StreamLine laboratory product, Singapore) to avoid contamination. The plates were covered, sealed and incubated at 37 °C overnight to check the sterility of plates and only sterile plates were further used in experiments.

Selected bacterial samples were taken out from −80 °C and kept in an ice box to prevent samples from thawing. Gram negative bacterial strains (Ten strains of PA and three strains of AB) were streaked on nutrient agar. Three strains of MRSA were grown on McConkey agar. Streaked plates were incubated for 16 h to allow bacterial colonies to grow. Antibacterial activity of AgNPs was determined through disc diffusion method. For disc diffusion assay, 0.9% of normal saline was prepared and 5 mL poured in sterile test tubes inside laminar hood. Single bacterial colonies from

streaked plates were picked using sterile loop and dropped into normal saline solution until turbidity of saline with bacterial inoculum was comparable to 0.5 McFarland Standard. Bacterial inoculum in normal saline was then swabbed using sterile cotton swabs on nutrient agar plates. Sterile filter paper discs of 6 mm diameter prepared from Whattman Filter Paper Grade 4 were placed on inoculated plates using a sterile syringe (BD 5 mL syringe, REF-305719, Becton and Dickinson, Pakistan) at the points marked up for each dilutions. 20 μL of each dilution of AgNPs (0.5–2.0 mg mL^{-1}) was dispensed on swabbed plates and allowed to get absorbed by filter paper discs. Antibiotic discs were placed on each plate which acted as positive control for the experiment. Deionized water and plant extracts (*Heliotropium crispum*) were used as negative controls. Plates were incubated overnight at 37 °C. Each experiment was repeated in twice.

2.2.4. Growth inhibition in liquid medium

Effect of 2.0 mg mL^{-1} AgNPs concentration on bacterial growth was observed through growth inhibition in liquid medium also. 50 μL of bacterial culture from different bacterial strains stored in glycerol stock solutions were grown in 5 mL of Luria Bertani (LB) Broth at 37 °C and at 200 rpm in shaking incubator. After 24 h, freshly grown 20 μL of bacterial inoculum with 10^4 log cells were transferred into 5 mL of LB broth. 20 μL of 2.0 mg mL^{-1} of AgNPs were added into the experimental tubes while control was left untreated. Bacterial culture was allowed to grow at 100 rpm, 37 °C for 24 h in shaking incubator. Optical Density (OD) of treated and untreated bacterial culture was measured at 600 nm after 24 h of incubation using Spectrophotometer (OPTIMA SP-300). OD_{600} of bacterial strains treated and untreated with AgNPs was compared and growth inhibiting effect of nanoparticles were noted. The experiment was repeated three times and mean values were recorded.

2.3. Anti-biofilm activity of silver nanoparticles

2.3.1. Biofilm inhibition and selection of strains

Bacterial strains of PA were checked for their biofilm forming potential by growing bacterial (50 μL) in 5 mL of LB Broth for 48 h in shaking incubator at 37 °C. LB broth was prepared according to the protocol of Sambrook et al. [44]. The PA bacterial strains that released green-blue pigment and showed visible signs of biofilm formation within 48 h were then selected for further studies. For biofilm inhibition studies, selected bacterial strains were grown in tryptone soya broth at 37 °C overnight (Fig. S1A & B).

2.3.2. 24 h AgNPs treatment in growth media

To judge the efficacy of AgNPs as biofilm inhibitory agent, 200 μL of freshly inoculated bacteria was added to 6-well microtitre plate. 1 × 1 cm cover slips acted as a substrate for biofilm formation. 100 μL of 1.5 mg mL^{-1} of AgNPs was added in one well along with bacterial inoculum while untreated microtitre well inoculated with same bacterial strain acted as a positive control for the experiment. The 6 well plate was allowed to incubate at 37 °C for 24 h. Coverslips were removed and washed with 1 × PBS inside laminar flow hood and fixed-samples were subjected to SEM analysis.

2.3.3. 72 h treatment with Ag-coated substrate

AgNPs were allowed to adsorb on a glass cover slip (Atlas, Italy), activated with 70% ethanol for 2–3 h. The 1 × 1 cm glass cover slips were left to air dry inside laminar flow hood. 50 μL of bacterial inoculum (strain no PA10 and PA20) grown overnight in TSB were taken out and dropped into 1 × 1 cm cover slip, which provides a substrate for biofilm formation and placed in 6 well Microtitre plates. Each strain was added in two wells of 6-well plates (SPL Life Sciences, Korea), one containing silver nanoparticle adsorbed coverslip while other containing untreated glass coverslip (control). 6 mL of fresh TSB was added over cover slips to provide while in last two wells TSB media without any inoculum was added which acted as a negative control. The 6-well plate was allowed to incubate at 28 °C for 72 h in static conditions. Coverslips were carefully removed with forceps after 72 h from microtitre plate well inside laminar flow hood and washed thoroughly with 1 × PBS to remove planktonic cells and prepared for SEM analysis.

2.3.4. SEM sample preparation for anti-biofilm assay and analysis

Cover slips subjected to biofilm inhibition assay were prepared and fixed for SEM analysis as followed: 4% Paraformaldehyde (PFA) was prepared which acts as a primary fixative. 100–200 μL of PFA was dropped onto each cover slip inside laminar flow hood and allowed to air dry for 30–45 min. Coverslips were carefully picked with forceps and samples were dehydrated by immersing for 2–3 min in chilled ethanol of increasing concentration i.e. 25–100%. Dried samples were sealed in sterile plastic petri plates and stored at 40 °C until subjected to SEM analysis. SEM and EDS analysis of samples were carried out and biofilm destruction as well as changes in morphology of bacterial cells treated with AgNPs compared with untreated bacterial samples after analysis. The SEM results of bacteria with and without treatment were analyzed for their morphology, shape and size with J-model 1.48 v software.

3. Results and discussion

3.1. Physicochemical optimization of AgNPs with corresponding SPR

We observed a rapid color change within 15 min in reaction mixture when *Heliotropium crispum* (HC) mediated synthesis of AgNPs was carried out. AgNPs when subjected to UV–vis Spectroscopy revealed the information regarding formation, size distribution, size, shape and the dielectric constant of AgNPs in colloidal aqueous solution [19]. For most of the optimized parameters studied, the maximum peak absorbance was detected at 430 nm wavelength. The absorbance peak observed is due to increased SPR of Ag following nanoparticle assembly. When excited by UV-radiations, the strong interaction of the AgNPs with light waves occurs due to collective oscillation of conduction electrons on the Ag surface. Therefore, single peak is indicative of regular morphology and stabilized nano-suspension. The UV–vis absorption spectrum wavelength range between 400 and 530 nm corresponds to spherical Ag morphology [20].

HC aqueous extract has strong reducing potential as a stable nano-fluid with dispersed AgNPs formulated within 30 min of all of the reaction conditions included in the study. Absence of SPR absorption peak between 400 and 800 nm for plant extract confirms that peak observed at 430 nm was due to AgNPs alone (Fig. S2 and XRF graphs Fig. S3). [21]. Size, shape and dielectric function of surrounding dispersed medium of synthesized AgNPs determine the strength of SPR of nanoparticles. Hence, it is important to control parameters to obtain desired size and shape of nanoparticles for biomedical applications [19].

The concentrations of aqueous extract that yielded stabilized nanoparticles was determined to control the assembly of nanoparticles. A broad UV-spectrum normalized curve was obtained at a reactant volume of 0.1 mL for each reaction concentration of plant. High level of absorption signals were obtained at 0.4 mL and 0.5 mL indicating that increased plant concentration provides increased reduction potential in the extract and results in compact packing of nanoparticles were observed in Fig. 1(a–c). Likewise, it was observed from UV-spectrum graphs that nanoparticles

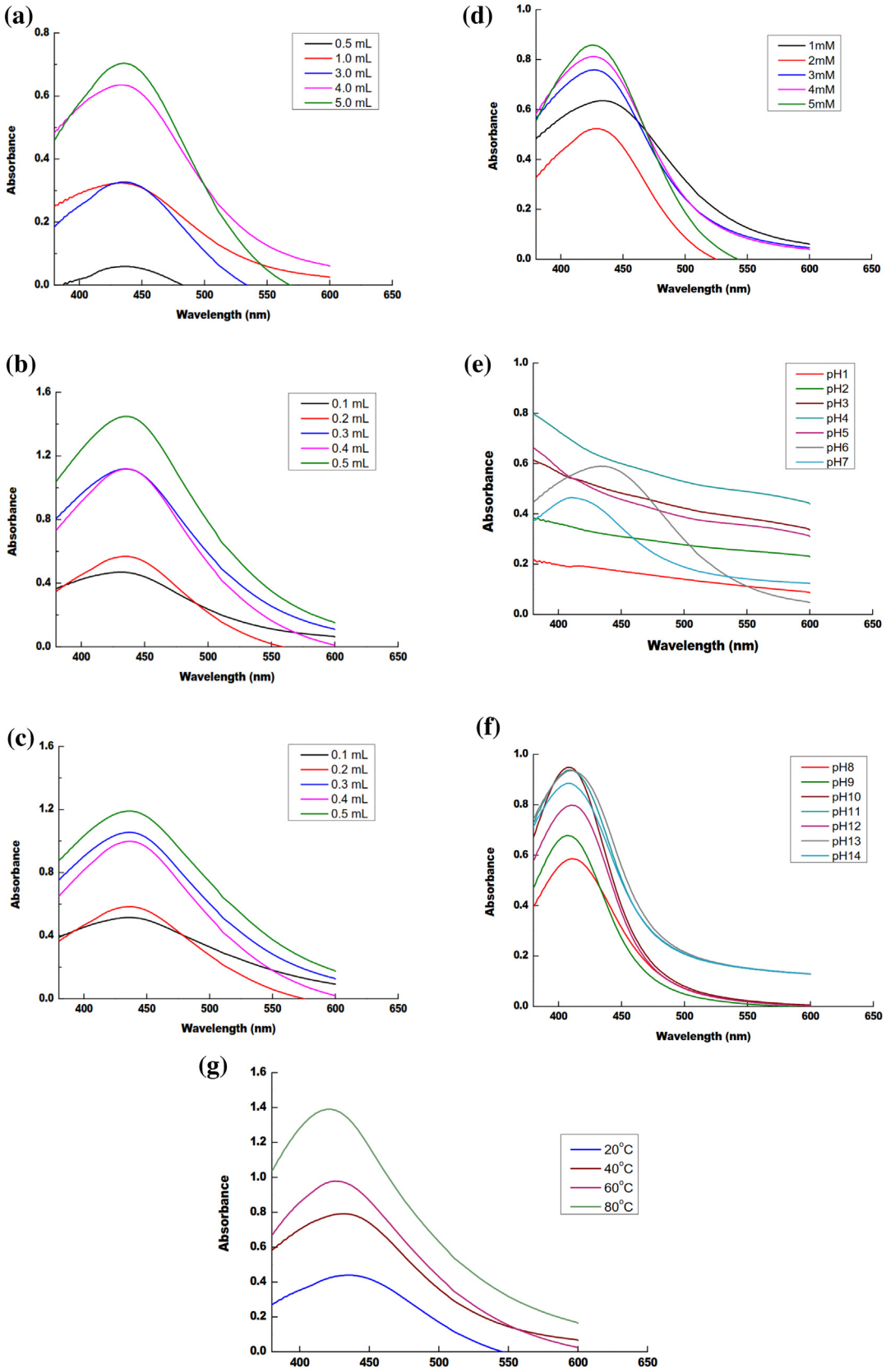

Fig. 1. Surface plasmon absorption spectrum of AgNPs following optimization of various physiochemical parameters to obtain stabilized low poly-dispersed nano-fluid. (a) Indicates UV–vis absorption spectrum at 0.5 μg mL^{-1} (b) 1.0 μg mL^{-1} and (c) 1.5 μg mL^{-1} of plant extract concentration. (d) Represents $AgNO_3$ (e) acidic pH (f) basic pH and (g) temperature dependent assembly of Ag nano-composite.

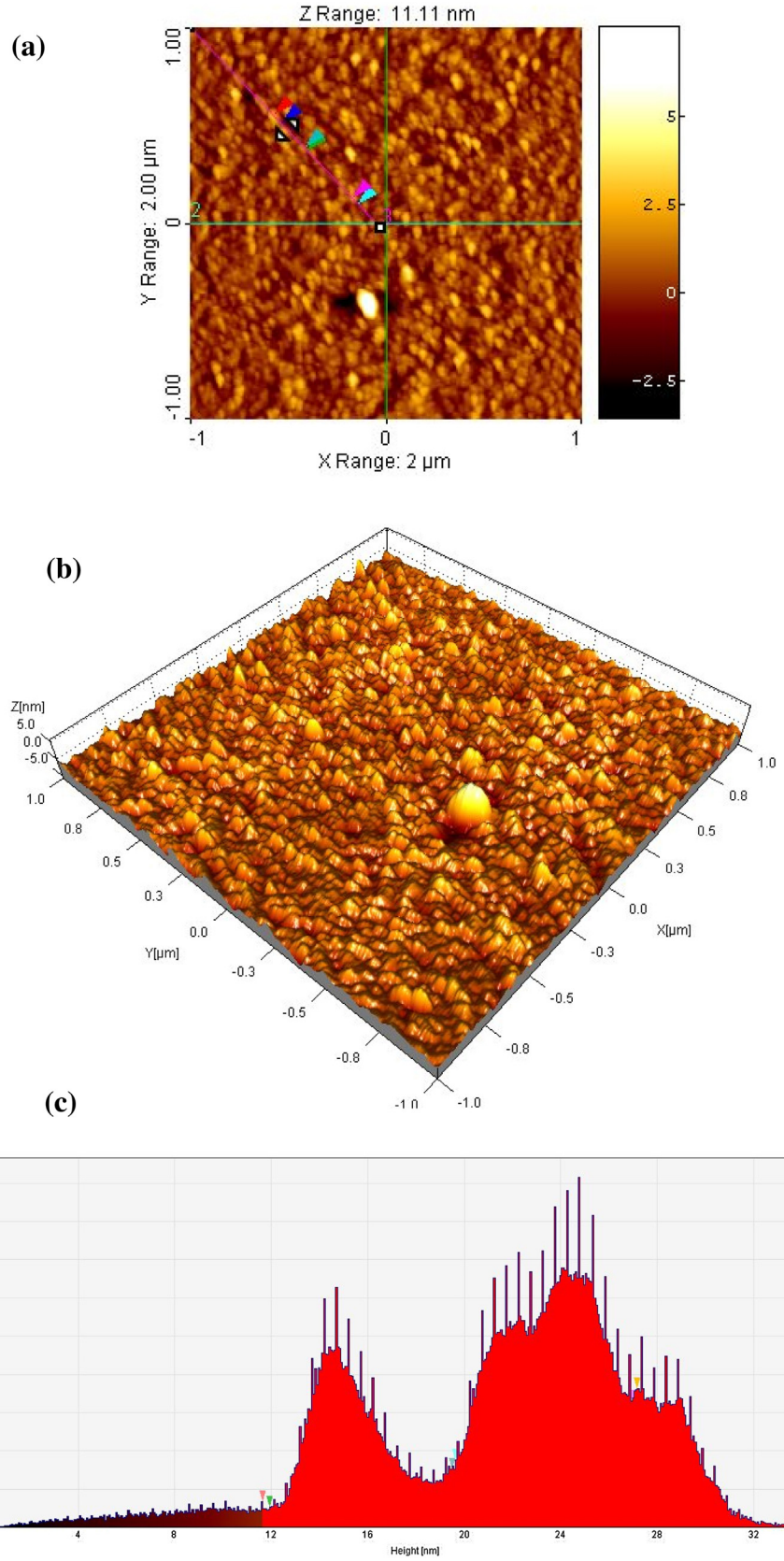

Fig. 2. Atomic force microscopy 2D and 3D images of AgNPs which provides information regarding size, morphology and shape of assembled NPs. (a) 2D AFM image of AgNPs. (a) 3D topographic AFM image of AgNPs (c) normal distribution graphs for calculation of average particle size and size distribution of assembled AgNPs from PSD map calculated through SPIP.

were formed at each of plant extract concentration i.e. 5 μg mL^{-1}, 10 μg mL^{-1} and 15 μg mL^{-1} in same UV range hence altering the extract concentration does not modulate the size, shape or formulation of AgNPs. The HC can act as an efficient biomaterial even when plant extract concentration is kept to a low concentration of 5 μg mL^{-1}, a factor advantageous for industrial upscale of AgNPs assembly.

The use of varying concentrations of poly-electrolytes and reducing agents at high temperatures to control the size of Ag nanoparticles have been reported in the past, hence a similar method was adopted in the current study [22,23]. We selected minimum concentration of plant extract (5 μg mL^{-1}) to study the effect of physicochemical parameters on nanoparticles formation. At 5 mM concentration of $AgNO_3$, comparatively high absorbance was obtained when compared with 1 mM of $AgNO_3$, but same absorption range, peak near 430 nm, implying that molarity of $AgNO_3$ does not affect SPR, shape or size range of formed AgNPs (Fig. 1d). The optimum pH of reactant mixture for stabilized dispersion of nano-fluid was found to be 6. At pH below 6, reduction of Ag ions to AgNPs did not take place implying denaturation of plant phytochemicals in acidic micro-environment that halted AgNPs assembly as observed in Fig. 1e. The low pH conditions formed nanoparticles with irregular spherical morphology such as in pH 6 which may be due to thicker capping agents shell around core silver nanoparticle [24]. At a basic pH of 8–14, nanoparticles, blue shift in absorption spectrum was observed for AgNPs synthesis showing an SPR wave length shift to 410 nm maximum absorbance from 430 nm. This indicates that smaller size nanoparticles were obtained at basic pH in comparison to acidic conditions, due to greater reduction rate of the functional group precursor in alkaline conditions. The wavelength range of AgNPs was also narrower such as in case of pH 14 indicating less polydispersed AgNPs formation (Fig. 1f).

At 20 °C reaction conditions, synthesized nanoparticles showed same wavelength range as in particles formed at 80 °C, but absorption peak was higher at 80 °C that can be an indication of increased AgNPs detection. This suggests that phytochemicals/protein factors involved in AgNPs self-assembly result effectively at a broad range of temperature, increasing ease of upscale of AgNPs synthesis at industrial level (Fig. 1g). HC mediated synthesis of AgNPs exhibited physicochemical dependent control of morphology, shape and size, a phenomenon in agreement with previous reports [20]. The SPR peak wavelength at 430 nm can be attributed to Mie scattering which responds only to silver metal [25,26].

3.2. Morphological characterization by AFM and SEM

The assembly of AgNPs under optimized conditions were evaluated for exact morphology, core size and shape through AFM. Scanned area for 2D image was 2 μm each at X and Y axis and size/height (Z-axis) range probed was 11.1 nm (Fig. 2a). The scanning probe surface for 3D topological view was estimated to be 5 nm as shown in Fig. 1b, suggesting maximum height of spherical particles to be of 11 nm on surface. AFM results provided surface evaluation of height of AgNPs (core size). Morphology and shape of nanoparticles were noted to be spherical, with intact smooth surface and few agglomerates visible in Fig. 2b, implying polydispersed nanoparticles. Further evaluation of average particle size from histograms was ranged between 4 and 32 nm in colloidal fluid as depicted in Fig. 2c.

Morphological characteristics and size of AgNPs were confirmed through SEM analysis. Fig. 3a shows SEM images depicting spherical nanoparticles, dispersed with uniform morphology. AgNPs were dispersed evenly in the loaded sample with few clusters presenting bead-like SEM micrographs. EDS results (Fig. 3b) confirm the presence of metallic silver in the sample concluding formation of AgNPs in HC extract. The SEM results suggested that AgNPs exhibited a size distribution between 30 and 50 nm. The nano-fluid with 40 nm average particle size can exhibit effective antibacterial properties since nanoparticles of size 30–40 nm present direct interaction with bacterial cell wall as reported in previous studies [27]. The bead like formation at fixed distances was due to interaction of functional groups attached with AgNPs, increasing the probability of strong electrostatic repulsion with other AgNPs in aqueous vicinity [28].

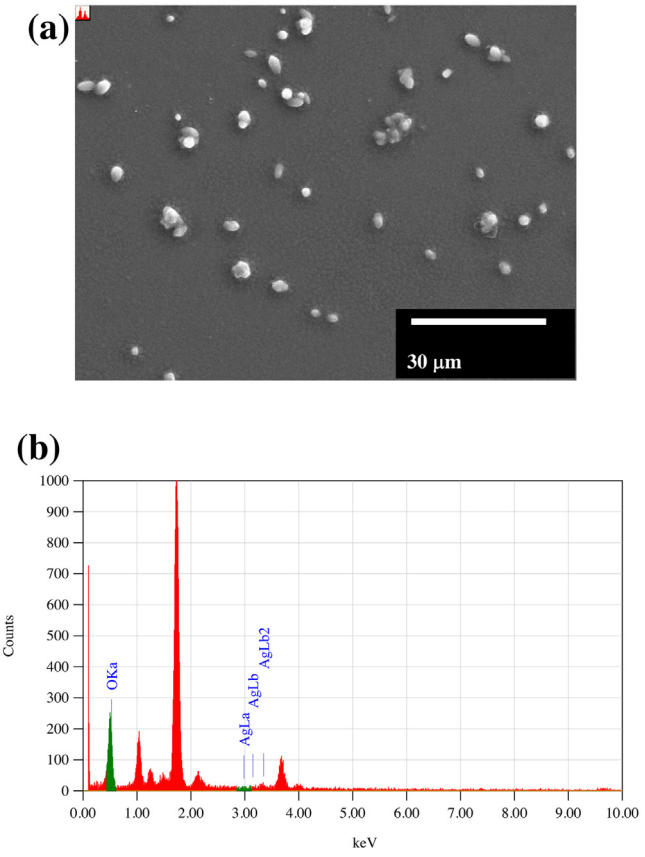

Fig. 3. Scanning Electron Microscopy images of assembled AgNPs. (a) SEM image at ×50,000 magnification revealing bead like uniform morphology of AgNPs and size ranged between 30 and 60 nm (b) Corresponding Energy Dispersive Spectroscopy graph confirming metallic silver presence at nano-metric range.

The distinct irregular spherical morphology was due to interaction of AgNPs to its plant extract- derived capping agents. Hydrogen bonding and electrostatic interaction between bio-organic molecules and silver nanocomposites ensured the clear morphology of each nanoparticle. The size determined through SEM analysis verifies our AFM results, which only detected core Ag and not capping agents, that larger particle size was perhaps due to difference in capping shell around AgNPs composites [21].

3.3. Zeta potential of AgNPs

Dynamic light scattering (DLS) was used to determine the hydrodynamic diameter (*dH*) of the AgNPs in colloidal suspension where *dH* corresponds to the core Ag diameter with plant derived capping-layer on the AgNPs. The peak 1 (*dH* with higher light scattering intensity of 94.4%) corresponds to 58 ± 23 nm diameter of nanoparticles while *z*-average (cumulative mean *dH* of the AgNPs) was recorded to be 42–120 nm (Fig. 4a). The poly-dispersity index (PDI) was also recorded which provided information about homogeneity of the sample. As PDI value was 0.284, less than PDI 0.5,

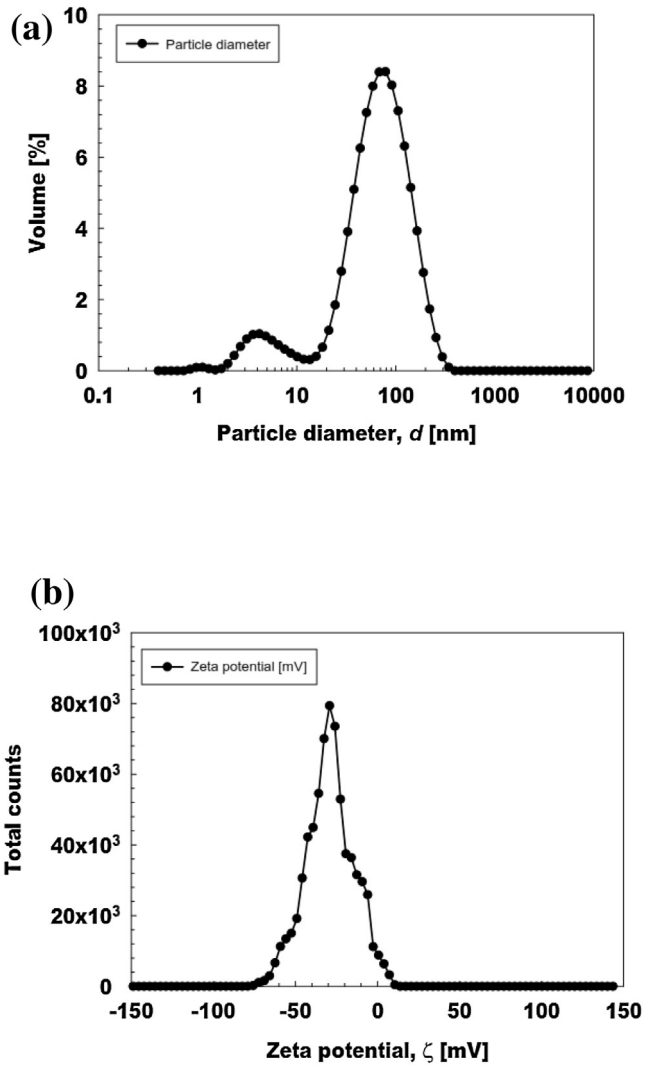

Fig. 4. (a) Particle size distribution of *Heliotropium crispum* AgNPs. (b) Zeta-potential of *Heliotropium crispum* loaded AgNPs.

the AgNPs were considered not to be aggregated (Fig. 4). The zeta potential of AgNPs at optimized pH 6 was found to be −29.3 mV, indicating a fair degree of stability of AgNPs in colloidal suspension (Fig. 4b). Zeta potential is correlated with AgNPs stability in colloidal suspension as zeta value greater than ±30 mV tend to be more stable with less agglomeration capacity. These correlations are significant for electrostatically capped nanoparticles [29] A similar report of negatively charged AgNps was made in the previous studies, indicating the ease of use of nanoparticles for various nanocomposite assembly and clear shell and core of AgNps detected following various synthesis methods (use of polyelectrolytes) [30]. The properties of shell are reported to correspond directly with the functionalization of composites and their applications such as nano-sensors [31].

3.4. Functional group assessment of AgNPs

The AgNPs were subjected to FTIR analysis to determine molecular micro-environment of AgNPs. During the biosynthesis of nanoparticles, functional groups present in the plant extracts were reduced and bounded with the nanoparticles to act as reducing, stabilizing and capping agents. FTIR was carried out on plant extracts before and after synthesis of nanoparticles and shift in chemical groups analyzed as a function of reducing agents for nanoparticle assembly. The FTIR analysis shows some changes in functional groups (Fig. 5a) and after synthesis of nanoparticles (Fig. 5b). Aqueous plant extract pellets shows various bond stretches at different wavelengths. 2030 cm^{-1} peak corresponds to nitrile bend (C≡N) while there was also evidence of amide group presence corresponded to peaks obtained at 1628 cm^{-1} and 3300 cm^{-1} respectively. The spectra showed a sharp and strong absorption band at 1628 cm^{-1n}assigned to the stretching vibration of (NH) C=O group. Phenol group (OH) stretch at 3473 cm^{-1} and tertiary amine (NH) stretch at 3300 cm^{-1} were also found (Fig. 5a). The Phenyl (C_6H_5OH) group presence was evident by the OH bond stretching along with the sp2 carbon bond stretching of C=C at 1628 cm^{-1}. Presence of NO_2 was also detected in the finger print region (1500–1000 cm^{-1}), where 1213 cm^{-1} represented the N=O stretch and the peak at 1040 cm^{-1} weak N—O bending. The 2 groups (N—H and C≡N) actively participated in the reduction of AgNPs as evident by peak shift in Fig. 5b.

Plant selection for nanoparticle synthesis is important as plant phytochemicals reduce and cap the Ag nano-composites. It has been reported from previous studies that polyol compounds and water soluble heterocyclic substances present in plant extract are responsible for reduction and stabilization of nanoparticles [32]. Polyol compounds refer to multiple hydroxyl groups containing compounds while heterocyclic compounds have organic carbocyclic components in cyclic form [33]. FTIR results suggest presence of amide and cyanide group in the plant extract indicating the phytochemicals were involved in the reduction of Ag^+ to Ag nanocomposites since these vibrational peaks were absent in synthesized nanoparticles. The presence of nitrate and nitrile group in plant extract suggests the strong reduction environment driving AgNPs assembly [21]. Furthermore, presence of phenyl peaks in our AgNPs sample suggests that polar groups surrounded assembled nanocomposites, explaining its solubility in aqueous suspension [34]. However, presence of hydrophobic alkyne C≡C chain group could explain few agglomerates as a result of interaction of functional groups [35]. This further verifies our AFM results findings in which metallic AgNPs were found as distinct spheres with few agglomerates formed due to components present in their micro-environment. A range of both polar and nonpolar groups as capping and stabilizing agents in nanoparticles were hence identified which controlled the nano-particles growth, stability and shape during synthesis process [36]. The FTIR analysis suggest enzymatic polymerization of plant-derived phenyl and alkyne groups on AgNPs. Plant derived multiple phenyl groups polymerize and adhere onto Ag surfaces. It has been reported in previous studies that such phenyl-group containing biomolecules provide polarity to the synthesized nanoparticles. It was observed from previous studies that alkylating groups passivate the nanoparticles [37] and presence of alkyne and phenyl chains can help to reduce cytotoxicity of AgNPs. Presence of capping agents also explain the need for high concentration of silver (2.0 mg mL^{-1}) required to induce potent bactericidal effect in the present study.

3.5. Anti-bacterial growth inhibition studies of AgNPs

The AgNPs were tested on highly pathogenic and multiple drug resistant strains of PA, MRSA and AB. The data of all the reported strains was recorded during the month of study which primarily represents the strains that were isolated from clinical settings at AFIP, Rawalpindi, Pakistan. The collected species were biochemically identified and characterized at AFIP according to its antibiotic resistance profile (Table S2–5). Antibacterial effect of synthesized AgNPs was checked against 10 strains of PA, 3 strains of MRSA and 3 strains of AB. Kirby-Bauer bacterial zone inhibition assay was carried out to determine the minimum concentration of AgNPs that could provide therapeutic effect against bacterial

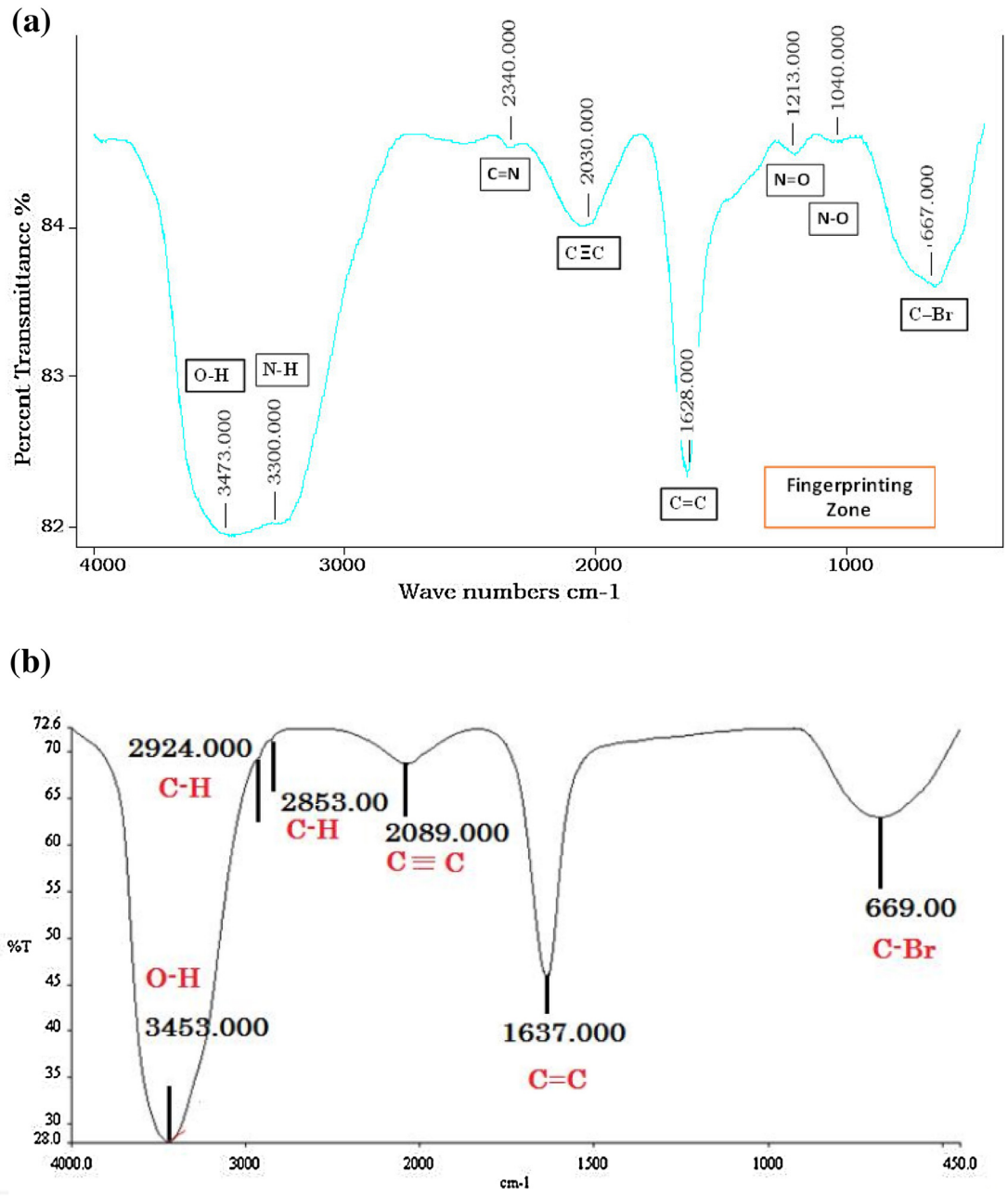

Fig. 5. FTIR analysis graphs showing percentage transmission of wavelength with corresponding wave numbers. (a) Identified functional groups in *Heliotropium crispum* aqueous plant extract pellet. (b) Silver nano-composite showing shift in functional groups and addition of new chemical bonds and functional groups following synthesis.

pathogens. Further a dose was adjusted which could provide maximum bactericidal response in culture broth. Mode of anti-biofilm and antibacterial effect of AgNPs was then made through SEM analysis of disrupted bacterial cells and biofilms.

The minimum inhibitory concentration (MIC) of AgNPs was found to be 0.5 mg mL^{-1} as concentration below that failed to produce significant zone of inhibition. The diameter of zone of inhibition increased with increase in concentration of AgNPs (Fig. 6a). It was observed that the nanoparticles were effective against all strains of PA, MRSA and AB tested and the difference in zone of inhibition recorded was dependent upon each strain not on type of bacterial specie selected. It was also observed that strains such as PA8 and PA12 which were showing resistance towards all ten antibiotics tested showed zone of inhibition of 17.5 mm and 16 mm each respectively, implying that antibiotic resistant strains were susceptible to AgNPs. Negative controls, deionized water and plant extracts showed no zone of inhibition indicating that the inhibiting diameter in treated strains was due to AgNPs alone (Fig. S4).

The maximum zone of inhibition diameter recorded at 2.0 mg mL^{-1} AgNPs concentration was 19 mm (MRSA 2) while minimum inhibitory diameter recorded was also against gram positive MRSA 4 (12 mm). PA and AB strains an average diameter of 16 mm at 2.0 mg mL^{-1} concentration of AgNPs was observed (Fig. 6a). The 2.0 mg mL^{-1} AgNPs concentration was taken as acceptable concentration to mediate a strong bactericidal effect as all assayed bacterial strains exhibited profound inhibitory zones at this concentration.

Two factors determined the bactericidal effect of synthesized AgNPs in present study, which in turn effected their therapeutic application as antimicrobial agents. First factor is the charge and

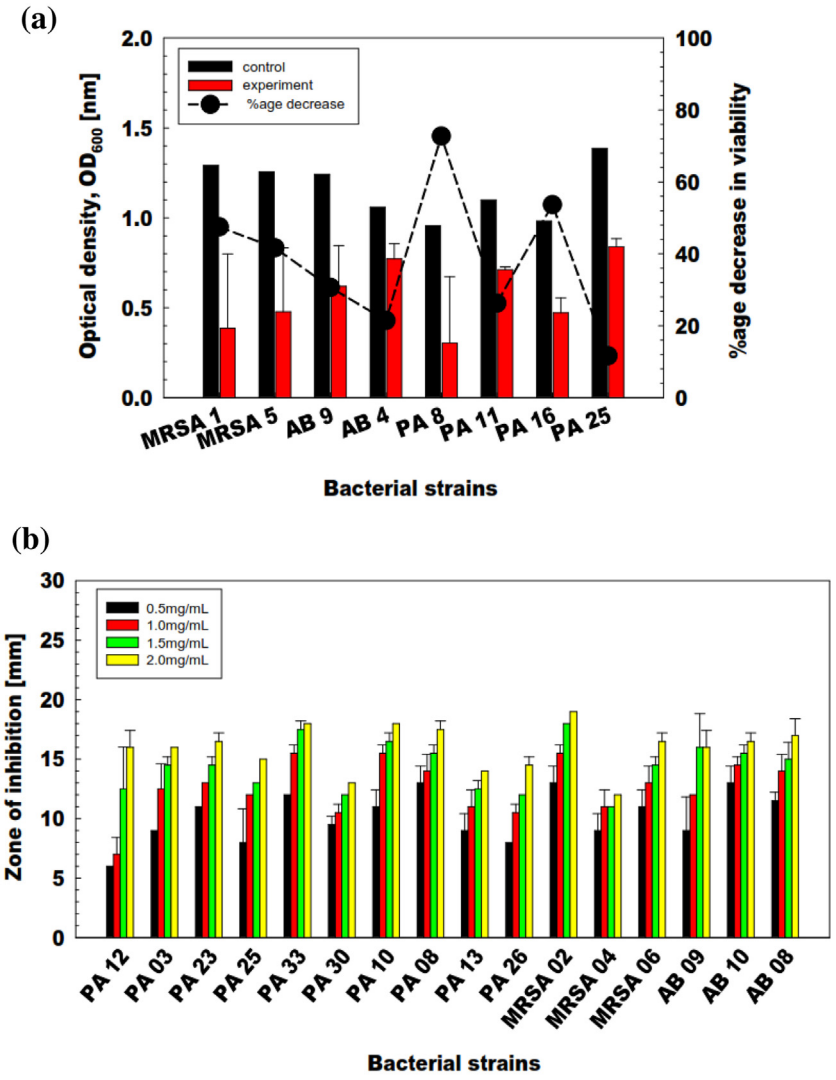

Fig. 6. Anti-bacterial inhibitory effect of AgNPs synthesized from *Heliotropium crispum*. (a) Diameter of zone of inhibition of strains after treatment with different concentration of silver nanoparticles is plotted in the figure. 0.5 mg mL^{-1} was noted as minimum inhibitory concentration while a significant inhibition zone was recorded for 2.0 mg mL^{-1} concentration. Mean difference in potency of AgNPs was observed for each bacterial strain and type, implicating *Heliotropium crispum* nanoparticles effect is specie independent. (b) Growth inhibition of bacterial strains at 24 h when treated with 2.0 mg mL^{-1} of AgNPs showed significant decrease in OD_{600} for each of the specie. *PA: *Pseudomonas aeruginosa*, MRSA: Multiple Drug Resistant *Staphylococcus aureus*, AB: *Acinetobacter baumanii.*

size-dependent and bactericidal effect of AgNPs which suggests that 40 nm size range provides Ag-bacterial cell direct interaction [27,38]. In another study it was reported that AgNPs in size range of 25 nm exhibit maximum bactericidal activity against a broad range of gram positive and gram negative bacteria [39] while AgNPs size range of <15 nm induce reactive oxidative stress in cellular milieu [40,41]. It was noted in the present study that antibacterial action of AgNPs is specie independent and strictly strain dependent as both Gram negative PA and AB and Gram positive MRSA exhibited differential inhibition zones and decrease in bacterial viability.

Growth inhibition pattern of selective strains of PA, MRSA and AB was monitored by measuring the OD_{600} of bacterial strains following 24 h incubation with highest effective dose (2.0 mg mL^{-1}) of AgNPs. Fig. 6b represents an analysis of nanoparticles treated versus untreated strains. The results show a significant decrease in OD_{600} for all three species of bacteria in different strains following incubation with AgNPs. Percentage decrease in bacterial viability was shown by black trend line in Fig. 6b implying that AgNPs at 2.0 mg mL^{-1} concentration cause growth inhibition between 10–70% depending upon the types of bacterial strains. Furthermore, the highest antibacterial activity was noted against PA (PA 8 and PA 16 strains showing 70%–50% decrease in viability following treatment). PA 8 and PA 16 strains were resistant to all the ten antibiotics tested hence, the results suggest that AgNPs mediate a sufficient bactericidal effect against resistant pathogens. We found that AgNPs were least effective against two strains of treated AB as 30% decrease in OD_{600} was observed for AB9 while 20% decrease was observed for AB4 strain. The growth inhibition results suggest that AgNPs mediated bactericidal effect was highly specie dependent and strain independent. Furthermore, the stability studies have been carried out on AgNPs using same method of synthesis. The data suggests that using higher plant concentration (increased from 1.5 mg mL^{-1} to 5 mg mL^{-1}), MIC of AgNPs decreased to 0.01 mg mL^{-1} of HC-AgNPs (Data not shown). Utilization of biocompatible polymers such as polyethylene glycol and poly vinyl pyruvate further decreased the MIC of *Heliotropium crispum* mediated assembled AgNPs (Data not shown, will be the part of second study).

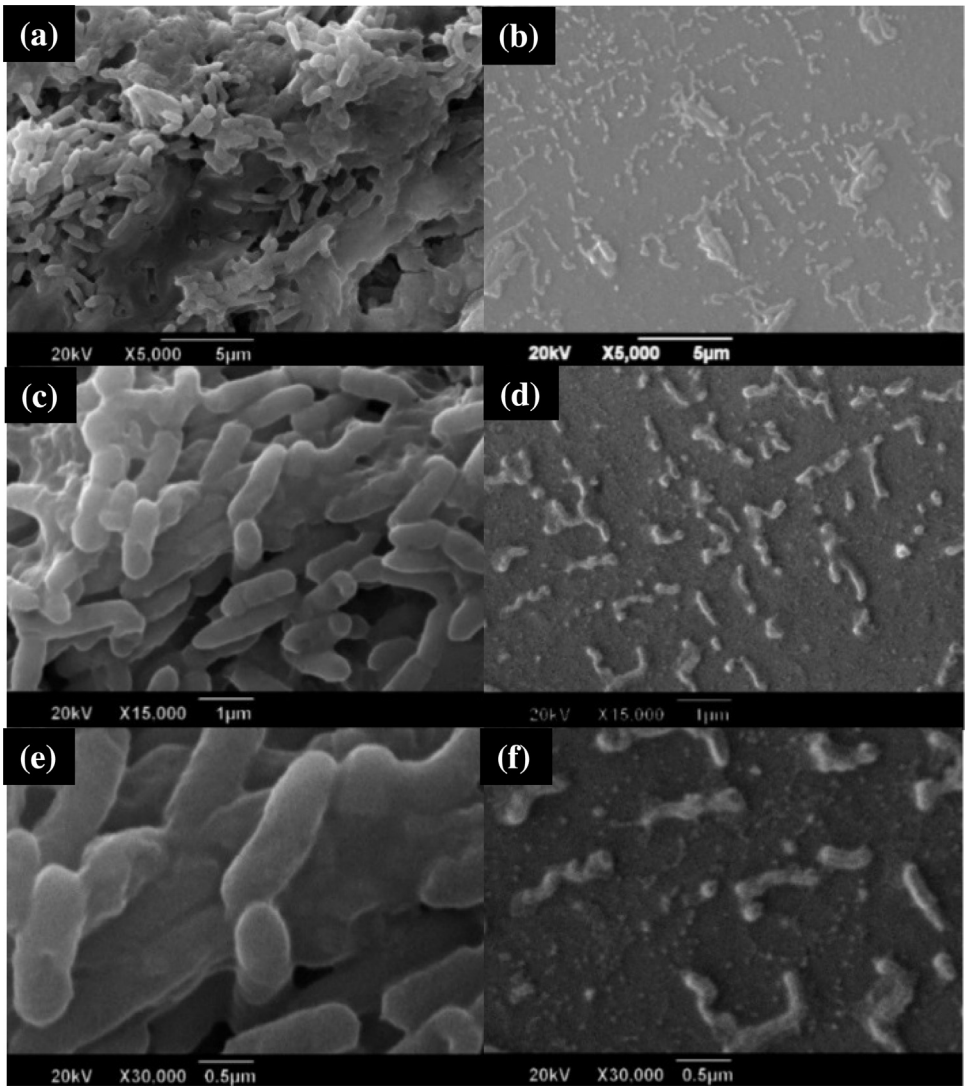

Fig. 7. SEM images of *Pseudomonas aeruginosa* exhibiting biofilm formation at 24 h with and without AgNPs treatment. (a, c, e). *P. aeruginosa* planktonic growth and colonization at 24 h without AgNPs treatment (control). (b, d, f) SEM images of *P. aeruginosa* after 24 h of treatment with AgNPs. Images at magnifications of ×5000, ×15,000 and ×30,000 were recorded in the study.

3.6. Anti-biofilm response of AgNPs

PA strains were incubated with AgNPs treated media to observe the effect of AgNPs on planktonic growth and biofilm production at 24 h (Fig. S6). HC-Ag nanoparticles mediated destruction of bacterial cells was revealed in captured SEM micrographs. Images in Fig. 7a, c and e shows bacterial biofilm production at 24 h in our control samples without AgNPs treatment. PA biofilm was at maturation phase following 24 h of growth. Gram negative rod shaped bacteria have colonized through secreted extracellular polymeric substances (EPS). It was clear that the morphology of bacteria remains intact in nanoparticles untreated substrate and the biofilm production process remains unimpeded. Note the intact morphology of individual bacterial cells at ×30,000 and mesh like structure exhibited due to binding between bacterial cells at lower magnifications of ×5000 and ×15,000 in Fig. 7c–f respectively.

AgNPs mediated disruption of bacterial biofilm and bactericidal effects at 24 h was exhibited in SEM micrographs in Fig. 7b, d and f at various magnifications. At magnifications of ×5000 and ×15,000 and ×30,000 a clear disruption of biofilm was observed. The EPS and peptidoglycan bonds that helps in bacterial colonization have been destroyed and changes in the morphology of bacteria were observed, which becomes more apparent when compared with untreated control samples. Presence of nano-metric scaled spherical AgNPs and destroyed organic debris was also observed in the bacterial vicinity, which were verified through EDS. Images of planktonic bacterial cells at ×15,000 and ×30,000 in Fig. 7d and f depicts a clear destruction of bacterial cell. Furthermore, morphology and shape of planktonic bacteria were changed significantly as a result of massive bactericidal effect of AgNPs (Fig. 7f).

SEM images were subjected to J-model software analysis provided an elaborated depiction of Ag nanoparticle's robust interaction with bacterial cell wall. The damaged cell wall and cellular debris in the background together with some nano sized AgNPs can be observed clearly in Fig. 8a,b. These micrographs suggest that AgNPs induces cell wall disruption through changing the permeability of peptidoglycan and lipoprotein components present in bacterial cell wall which then helps in massive destruction of biofilm through distorted morphology of bacterial cells as depicted in difference in bacterial morphology The electron diffraction peak of Ag obtained from planktonic bacteria in Fig. 8c shows that Ag was adsorbed on cell wall surface which in turn caused the damage

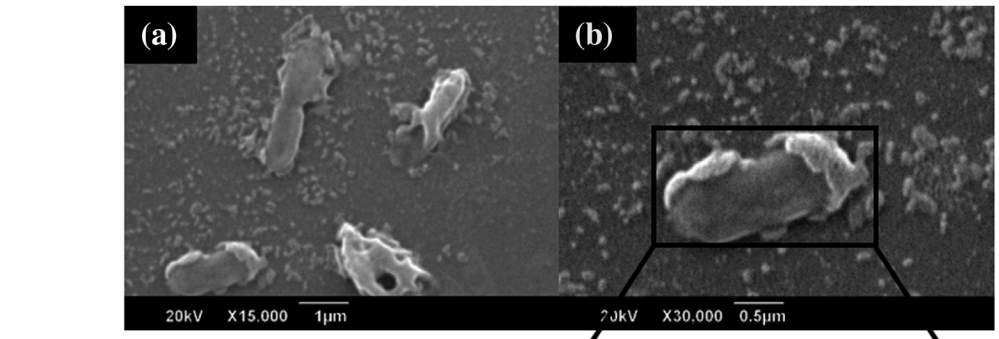

(c)

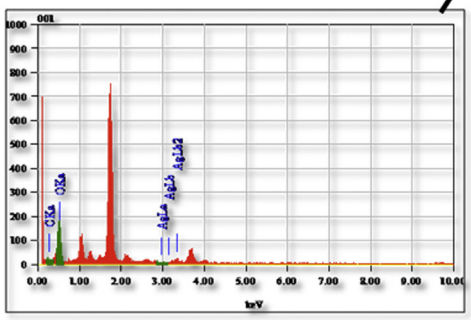

EDS Elemental Percentage

Element	Mass%	Atom%	Compound Mass%
C K	5.61	7.36	1.30
O K	94.05	92.59	98.53
Ag L	0.34	0.05	0.17
Total	100.00	100.00	100.00

(d)

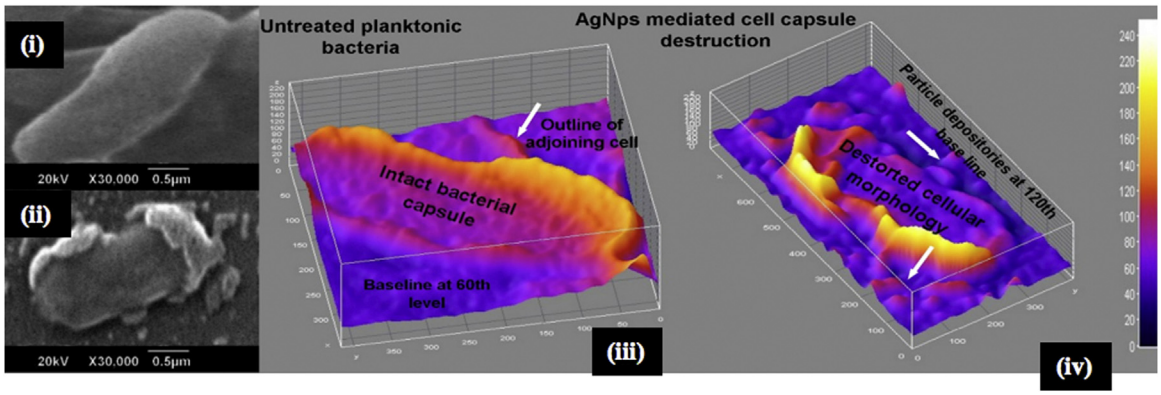

Fig. 8. Analysis of untreated and AgNPs treated bacterial cell images at 24 h through EDS and J-model interactive 3D analysis plot. (a,b) SEM images of planktonic bacterial cells with destroyed cell wall capsule and distorted morphology following AgNPs treatment at ×30,000 magnification. (c) EDS graph of bacterial cell debris from SEM image exhibiting the compositional analysis to confirm the presence of organic matter and AgNPs. The graph peak confirmed the elementary presence of silver that caused the destruction of planktonic bacterial with almost 0.17% compound mass percentage in destroyed region as displayed in the EDS table. (d) SEM micrographs of individual bacterial cells subjected to interactive 3D J-model analysis to study morphology of (i) untreated bacterial cell (×30,000) (ii) AgNPs treated bacterial cell (×30,000). (iii) Bacterial cell in untreated sample depicts smooth morphology and intact shape in 3D interactive graphs derived from SEM micrograph. (iv) AgNPs mediated destruction of planktonic bacterial wall exhibits irregular morphology in 3D plot, presence of cellular debris at 100th base line level and small particles at 80–120th baseline level on destructed cell was also observed.

in peptidoglycan linkages in bacterial cell wall. Compositional analysis through EDS depicts that in the selected region of Ag treated planktonic bacteria only a small concentration of silver i.e. 0.34% by mass can result in massive destruction of cell wall which in turn induced Ag-mediated bactericidal effect as observed in Fig. 8c.

Ag nanoparticle treated cell in Fig. 8d(*iv*) depicts the presence of irregular depressions on cell surface with apparent distortions in morphology. Maximum height of bacteria was at 200 scale showing sloughing-off of cell wall membranes, hence pronounced trough was observed. Presence of small particle-like troughs at 120th scale, marked by arrows, both inside and outside treated cells suggests particles of equal size are adsorbed on the bacterial cell and present in its vicinity. This suggests that AgNPs concentrated in the bacterial vicinity resulting in call wall collapse. However, regular morphology of treated bacteria suggests that at 24 h AgNPs mediated cell wall destruction has initiated but bacterial capsule is preserved. When compared with AgNPs untreated control in Fig. 8d(*iii*) it was noticed that bacterial cell was present at almost uniform height of 60–120th *z*-scale while Ag-treated bacteria in Fig. 8d(*iv*) exhibited more troughs due to distorted morphology hence height range

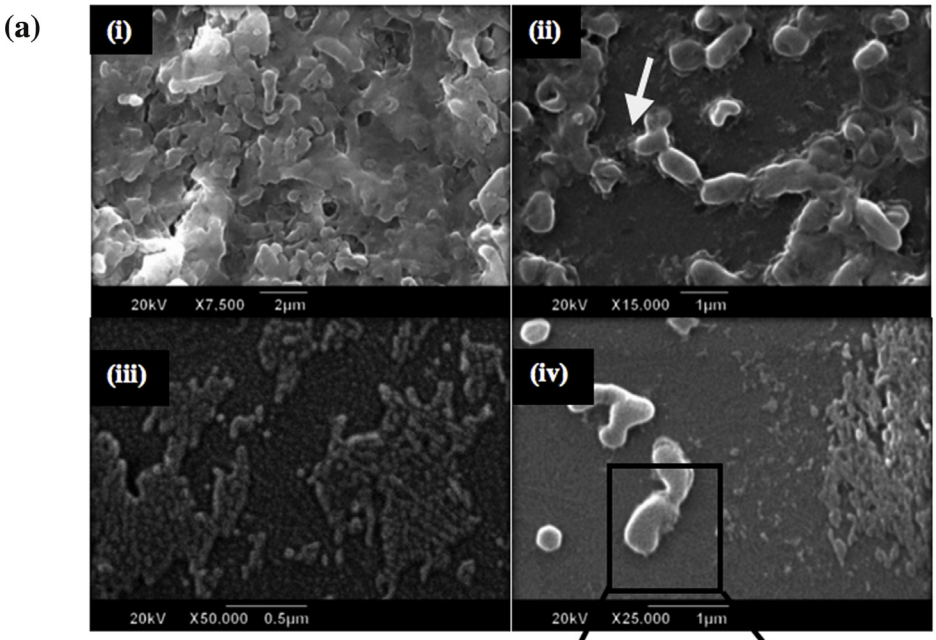

(b)

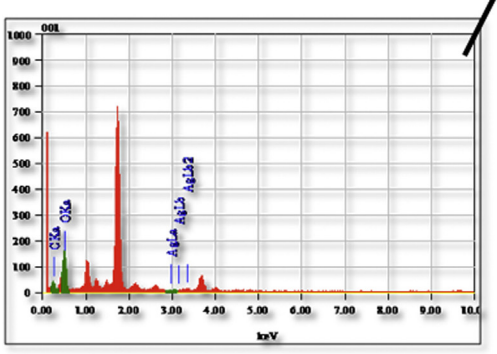

EDS Elemental Percentage

Element	Mass%	Atom%	Compound Mass%
C K	14.85	19.02	5.64
O K	84.09	80.83	93.54
Ag L	1.06	0.15	0.82
Total	100.00	100.00	100.00

(c)

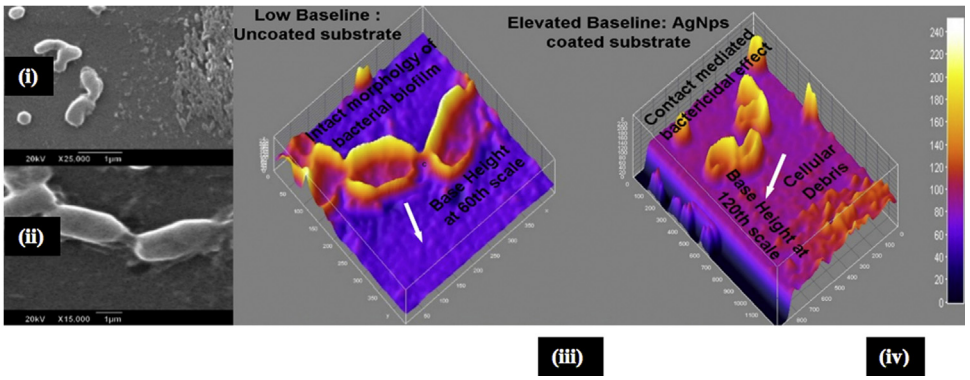

Fig. 9. SEMs of *Pseudomonas aeruginosa* biofilm when grown on AgNPs coated substrate for 72 h. Corresponding EDS graph and interactive 3D plot by J-model provides an insight into biofilm destructive potential of *Heliotropium crispum* AgNPs. (a) SEM images of treated and untreated glass substrate at 72 h (i) *Pseudomonas aeruginosa* biofilm after 72 h, when no AgNPs treatment was given. Mature biofilm growth observed at ×7500 (ii) Planktonic cell dispersion from mature biofilm for further biofilm growth with clear EPS linkages between two bacterial cells at ×15,000. (iii) No bacterial growth exhibited on AgNPs coated glass substrate at ×50,000 following 72 h incubation. Note the presence of Ag nano composites deposited on glass. (iv) Immediate bactericidal effect is observed upon planktonic bacteria in contact with Ag-coated glass substrate for 72 h depicted at ×25,000. (b) EDS analysis of biofilm debris confirming presence of organic matter in sample with corresponding concentration of AgNPs. Almost 0.82% of Ag as a compound mass indicates the elementary silver presence resulting in a potent bactericidal effect at 1 μm region of bacterial cell vicinity (c) 3D interactive J model plot of planktonic bacterial cells at 72 h. (i)Bactericidal effect of Ag-coated substrate. (ii) SEM of biofilm formed following 72 h growth in untreated substrate. (iii) 3D plot of untreated substrate shows low substrate baseline and intact cellular biofilm following 72 h incubation. (iv) 3D plot of bacterial debris following 72 h incubation on AgNPs coated substrate showing a distinct layer of nanoparticles due to elevated baseline when compared with control. Also there is evidence of completely distorted bacterial biofilm.

varied from 60–220th *z*-scale. Absence of particle depressions in untreated control Fig. 8d(*iii*) suggests them to be AgNPs agglomerates in Fig. 8d(*iv*).

Glass substrate without adsorbed AgNPs showed significant biofilm growth at 72 h as shown in Fig. 9a(*i*) and (*ii*). Mature biofilm was evident with some planktonic bacterial dispersion visible from mature biofilm matrix following 72 h of incubation. There were also clear signs of matrix formed as a result of secreted EPS. Mature biofilm growth involves induction of quorum sensing molecules which then results in bacterial colonization. In Fig. 9a(*ii*) bacterial linkages through secreted EPS was observed (marked by an arrow). Clear and intact bacterial cell wall and maintained cell morphology are important features of our control sample.

SEM analysis of PA following incubation with AgNPs adsorbed glass substrate exhibited potent anti-biofilm and robust bactericidal effect even at 72 h of incubation (Fig. 9a (*iii)* & (*iv*)). AgNPs adsorbed glass substrate depict presence of bead-like structures of nanoparticles. The bacteria coming into direct contact with AgNPs impregnated surface are immediately lysed as observed in Fig. 9a(*iv*). EDS graphs obtained confirms the presence of silver on the glass substrate (Fig. 9b) while carbon and oxygen components represent the presence of debris of PA following Ag nanocomposite mediated massive destruction. EDS peaks further revealed that 0.82% by mass of AgNPs adsorbed at 1 μm region of substrate was highly potent even after 72 h of incubation (Fig. 9b).

Interactive 3D J model plot of AgNPs impregnated glass validated our findings. Presence of silver exhibited irregular bacterial morphology and high fragmentations of destroyed peptidoglycan, dispersed in the vicinity. The height of dispersed and destroyed organic matter (marked with arrow) in Ag-coated substrate was same as the destroyed bacterial cell i.e. at 200–220th scale level as shown in Fig. 9c(*iv*). The morphology of bacterial cells appear irregular and distorted following contact with Ag-adsorbed glass in Fig. 9c(*iv*). In untreated glass substrate (control) the morphology of bacterial cells appear uniform with intact capsule and peptidoglycan linkages between adjoining cells as depicted in Fig. 9c(*iii*). It was also observed that in Ag-treated glass substrate base height is at 100–120th z-scale level while in Ag-untreated glass, the base height is at 60–80th scale. This suggests the presence of Ag-nano composites as substrate coating agents hence resulting in base elevation when compared with control sample.

Many mechanisms of Ag-bacterial interaction have been proposed which includes attachment with thiol groups in bacterial enzyme, intercalation with negatively charged DNA, release of Ag^{+} ions in colloidal silver solution to bind and interfere with cell wall synthesis, cell membrane destruction via induction of reactive oxidation stress through free radicals [28,42]. However, the exact mechanism and mode of action of AgNPs on bacterial cells depend entirely upon size, shape, charge and capping ligands [6]. HC-AgNPs exhibited time and size dependent bactericidal and anti-biofilm effect. Bacterial capsule and cell membrane remained undamaged which suggests that nanoparticles initially caused peptidoglycan breakage in cell wall at 24 h, which in turn produced potent bactericidal response.

Effect of biofilm inhibitory action of AgNPs also remains unresolved. It is suggested from previous studies that Ag nanocomposites evoke a bacterial defense mechanism, "DNA conglomeration defense mechanism" which then slows down bacterial replication to minimize Ag toxic effect [43]. Biofilm formation process slows down as a defensive mechanism by bacteria, effectively reducing colonization. AgNPs can now rapidly evoke a potent bactericidal response against planktonic bacterial cells. The study confirms this hypothesis as our SEM micrographs at 72 h show only planktonic cell dispersions and robust AgNPs response.

4. Conclusions

Our study demonstrates the use of *Heliotropium crispum* plant extract as an efficient biomaterial for AgNPs synthesis. Plant extract concentration was found to be the most important parameter which directly effects nanoparticle composition by controlling size, shape and stability. Presence of plant-derived phytochemicals and functional groups can present unique optical and pharmacophore properties to bioengineered nanoparticles as exhibited by fluorescence potential and antibiofilm responses of HC-AgNPs. All clinical isolates of bacterial pathogen tested against HC-AgNPs were found to be susceptible suggesting an efficient use of Ag nanocomposites to address emerging issue of multiple drug resistance in bacterial strains. Finally the results imply that AgNPs of 40 nm spherical morphology present potent bactericidal response through cell wall destruction. The HC-AgNPs loaded products can control multiple drug resistant pathogen spread in future.

Conflicts of interests

All authors declare that they have no conflicts of interests.

Acknowledgements

We acknowledge ASAB NUST for providing us with research facilities for this project. We are also thankful to SCME NUST and Department of Chemistry LUMS for facilitating us with various analytical analysis for this study.

Appendix A. Supplementary data

Supplementary data associated with this article can be found, in the online version, at http://dx.doi.org/10.1016/j.apsusc.2016.05.133.

References

[1] R. Behra, L. Sigg, M.J. Clift, F. Herzog, M. Minghetti, B. Johnston, A. Petri-Fink, B. Rothen-Rutishauser, Bioavailability of silver nanoparticles and ions: from a chemical and biochemical perspective, J. R. Soc. Interface 10 (2013) 20130396.
[2] M.A. Dar, A. Ingle, M. Rai, Enhanced antimicrobial activity of silver nanoparticles synthesized by *Cryphonectria* sp. evaluated singly and in combination with antibiotics, Nanomedicine 9 (2013) 105–110.
[3] C. Marambio-Jones, E.V. Hoek, A review of the antibacterial effects of silver nanomaterials and potential implications for human health and the environment, J. Nanopart. Res. 12 (2010) 1531–1551.
[4] L. Wei, J. Lu, H. Xu, A. Patel, Z.-S. Chen, G. Chen, Silver nanoparticles: synthesis, properties, and therapeutic applications, Drug Discov. Today 20 (2015) 595–601.
[5] P. Narayanan, W.S. Wilson, A.T. Abraham, M. Sevanan, Synthesis, characterization, and antimicrobial activity of zinc oxide nanoparticles against human pathogens, BioNanoScience 2 (2012) 329–335.
[6] P. Mohanpuria, N. Rana, S. Yadav, Biosynthesis of nanoparticles: technological concepts and future applications, J. Nanopart. Res. 10 (2008) 507–517.
[7] M. Gericke, A. Pinches, Biological synthesis of metal nanoparticles, Hydrometallurgy 83 (2006) 132–140.
[8] P. Logeswari, S. Silambarasan, J. Abraham, Ecofriendly synthesis of silver nanoparticles from commercially available plant powders and their antibacterial properties, Scientia Iranica 20 (2013) 1049–1054.
[9] J. Song, B. Kim, Rapid biological synthesis of silver nanoparticles using plant leaf extracts, Bioprocess Biosyst. Eng. 32 (2009) 79–84.
[10] S.P. Chandran, M. Chaudhary, R. Pasricha, A. Ahmad, M. Sastry, Synthesis of gold nanotriangles and silver nanoparticles using aloevera plant extract, Biotechnol. Prog. 22 (2006) 577–583.
[11] D. MubarakAli, N. Thajuddin, K. Jeganathan, M. Gunasekaran, Plant extract mediated synthesis of silver and gold nanoparticles and its antibacterial activity against clinically isolated pathogens, Colloids Surf. B 85 (2011) 360–365.
[12] H. Bar, D.K. Bhui, G.P. Sahoo, P. Sarkar, S.P. De, A. Misra, Green synthesis of silver nanoparticles using latex of *Jatropha curcas*, Colloids Surf. A 339 (2009) 134–139.
[13] D. Jain, H.K. Daima, S. Kachhwaha, S.L. Kothari, Synthesis of plant-mediated silver nanoparticles using papaya fruit extract and evaluation of their anti microbial activities, Dig. J. Nanomater. Biostruct. 4 (2009) 557–563.

[14] D. Yeo, B. Attioua, C. Lehalle, M. Kossi, J.D. N'guessan, A.J. Djaman, A. Lobstein, N. Frossard, Isolation of wound healing compounds from *Heliotropium indicum*, J. Appl. Pharm. Sci 10 (2011) 102–106.
[15] GlobinMed. *Heliptropium indcium*, www.globinMed.com. (assessed on 20.09.14).
[16] P.P. Fu, Q. Xia, G. Lin, M.W. Chou, Pyrrolizidine alkaloids—genotoxicity, metabolism enzymes, metabolic activation, and mechanism, Drug Metab. Rev. 36 (2004) 1–55.
[17] Y.N. Nasir, Heliotropium crispum, in: Tropicos (Ed.), Flora of Pakistan, Tropicos, 2011.
[18] C.H. Bosch, Heliotropium ramosissimum (Lehm.) DC, in: G.H. Schmelzer, A. Gurib-Fakim (Eds.), Prota 11(1): Medicinal Plants/Plantes médicinales 1, PROTA, PROTA, Wageningen, Netherlands, 2006.
[19] D.K. Bhui, H. Bar, P. Sarkar, G.P. Sahoo, S.P. De, A. Misra, Synthesis and UV–vis spectroscopic study of silver nanoparticles in aqueous SDS solution, J. Mol. Liquid 145 (2009) 33–37.
[20] J. Pranay, A. Vibhor, Synthesis, characterization and antimicrobial effects of silver nanoparticles from microorganisms—a review, Int. J. Nano Mater. Sci. 1–2 (2012) 108–120, Modern Scientific Press.
[21] P. Devaraj, P. Kumari, C. Aarti, A. Renganathan, Synthesis and characterization of silver nanoparticles using cannonball leaves and their cytotoxic activity against MCF-7 cell line, J. Nanotechnol. 2013 (2013) 5.
[22] X. Sun, Y. Luo, Preparation and size control of silver nanoparticles by a thermal method, J. Mater. Lett. 59 (2005) 3847–3850.
[23] W. Lu, F. Liao, Y. Luo, G. Chang, X. Sun, Hydrothermal synthesis of well-stable silver nanoparticles and their application for enzymeless hydrogen peroxide detection, J. Electrochim. Acta 56 (2011) 2295–2298.
[24] B.J. Wiley, S.H. Im, Z.-Y. Li, J. McLellan, A. Siekkinen, Y. Xia, Maneuvering the surface plasmon eesonance of silver nanostructures through shape-controlled synthesis, J. Phys. Chem. B 110 (2006) 15666–15675.
[25] E.G. Goh, X. Xu, P.G. McCormick, Effect of particle size on the UV absorbance of zinc oxide nanoparticles, Scr. Mater. 78–79 (2014) 49–52.
[26] S. Daniel, S. Ayyappan, N.J.P. Philiphan, M. Sivakumar, G. Menaga, T.A. Sironmani, Green synthesis and transfer of silver nanoparticles in a food chain through Chiranamous Larva to zebra fish—a new approach for therapeutics, Int. J. Nanosci. Nanotechnol. 2 (2011) 159–169.
[27] J.R. Morones, J.L. Elechiguerra, A. Camacho, K. Holt, J.B. Kouri, J.T. Ramírez, M.J. Yacaman, The bactericidal effect of silver nanoparticles, Nanotechnology 16 (2005) 2346.
[28] V.K. Sharma, R.A. Yngard, Y. Lin, Silver nanoparticles: green synthesis and their antimicrobial activities, Adv. Colloid Interface Sci. 145 (2009) 83–96.
[29] T. DeLuca, M. Kaszuba, K. Mattison, Optimizing silicone emulsion stability using zeta potential, American Laboratory News, 2006.
[30] S. Liu, J. Tian, L. Wang, H. Li, Y. Zhang, X. Sun, Stable aqueous dispersion of graphene nanosheets: noncovalent functionalization by a polymeric reducing agent and their subsequent decoration with Ag nanoparticles for enzymeless hydrogen peroxide detection, J. Macromol. ACS 43 (2010) 10078–10083.
[31] Y. Zhang, L. Wang, J. Tian, H. Li, Y. Luo, X. Sun, Ag@poly(m-phenylenediamine) core-shell nanoparticles for highly selective, multiplex nucleic acid detection, Langmuir 27 (2011) 2170–2175.
[32] J. Huang, Q. Li, D. Sun, Y. Lu, Y. Su, X. Yang, H. Wang, Y. Wang, W. Shao, N. He, Biosynthesis of silver and gold nanoparticles by novel sundried *Cinnamomum camphora* leaf, Nanotechnology 18 (2007) 105104.
[33] W. Reusch, Heterocyclic compound, in: Virtual Textbook of Organic Chemistry, Department of Chemistry, Michigan State University, East Lansing, MI, USA, 1999.
[34] M. Esfandyari-Manesh, S. Mostafavi, R. Majidi, M. Koopaei, N. Ravari, M. Amini, B. Darvishi, S. Ostad, F. Atyabi, R. Dinarvand, Improved anticancer delivery of paclitaxel by albumin surface modification of PLGA nanoparticles, DARU J. Pharm. Sci. 23 (2015) 28.
[35] S. Honary, P. Ebrahimi, H. Rad, M. Asgari, Optimization of preparation of chitosan-coated iron oxide nanoparticles for biomedical applications by chemometrics approaches, Int. Nano Lett. 3 (2013) 48.
[36] R.R. Naik, S.J. Stringer, G. Agarwal, S.E. Jones, M.O. Stone, Biomimetic synthesis and patterning of silver nanoparticles, Nat. Mater. 1 (2002) 169–172.
[37] M. Nakamoto, M. Yamamoto, M. Fukusumi, Thermolysis of gold (I) thiolate complexes producing novel gold nanoparticles passivated by alkyl groups, Chem. Commun. (2002) 1622–1623.
[38] J. Park, D.-H. Lim, H.-J. Lim, T. Kwon, J.-s. Choi, S. Jeong, I.-H. Choi, J. Cheon, Size dependent macrophage responses and toxicological effects of Ag nanoparticles, Chem. Commun. 47 (2011) 4382–4384.
[39] A. Panáček, L. Kvitek, R. Prucek, M. Kolar, R. Vecerova, N. Pizurova, V.K. Sharma, T.j. Nevečna, R. Zboril, Silver colloid nanoparticles: synthesis, characterization, and their antibacterial activity, J. Phys. Chem. B 110 (2006) 16248–16253.
[40] C. Carlson, S. Hussain, A. Schrand, L.K. Braydich-Stolle, K. Hess, R. Jones, J. Schlager, Unique cellular interaction of silver nanoparticles: size-dependent generation of reactive oxygen species, J. Phys. Chem. B 112 (2008) 13608–13619.
[41] D.F. Emerich, C.G. Thanos, The pinpoint promise of nanoparticle-based drug delivery and molecular diagnosis, Biomol. Eng. 23 (2006) 171–184.
[42] M. Sathishkumar, A. Mahadevan, S. Pavagadhi, R. Kaushik, V.K. Sharma, R. Balasubramanian, Biological synthesis of silver nanoparticles and assessment of their bactericidal activity Sustainable Nanotechnology and the Environment: Advances and Achievements, vol. 1124, American Chemical Society, 2013, pp. 107–120.
[43] K. Markowska, A.M. Grudniak, K.I. Wolska, Silver nanoparticles as an alternative strategy against bacterial biofilms, Acta Biochim. Pol. 60 (2013) 523–530.
[44] J. Sambrook, E.F. Fritschi, T. Maniatis, Molecular Cloning: A Laboratory Manual, Cold Spring Harbor Laboratory Press, New York, USA, 1989.